

1 **A binomial stochastic framework for efficiently**
2 **modeling discrete statistics of convective populations**

3 **R. A. J. Neggers¹ and P. J. Griewank¹,**

4 ¹Institute for Geophysics and Meteorology, University of Cologne, Germany.

5 **Key Points:**

- 6 • An efficient scale-aware stochastic number generator based on a Bernoulli process
7 is applied to model object births and advection on Eulerian grids.
- 8 • Discreteness in object number is conserved, while an age dimension is included to
9 represent evolution of object demographic strata.
- 10 • Population subsampling effects in the convective grey zone are reproduced, while
11 simple applications capture behavior as observed in nature.

Corresponding author: R. A. J. Neggers, neggers@meteo.uni-koeln.de

Abstract

Understanding cloud-circulation coupling in the Trade wind regions, as well as addressing the grey zone problem in convective parameterization, requires insight into the genesis and maintenance of spatial patterns in cumulus cloud populations. In this study a simple toy model for recreating populations of interacting convective objects as distributed over a two-dimensional Eulerian grid is formulated to this purpose. Key elements at the foundation of the model include i) a fully discrete formulation for capturing binary behavior at small population sample sizes, ii) object demographics for representing life-cycle effects, and iii) a prognostic number budget allowing for object interactions and co-existence of multiple species. A primary goal is to optimize the computational efficiency of this system. To this purpose the object birth rate is represented stochastically through a spatially-aware Bernoulli process. The same binomial stochastic operator is applied to horizontal advection of objects, conserving discreteness in object number. Implied behavior of the formulation is assessed, illustrating that typical powerlaw scaling in the internal variability of subsampled convective populations as found in previous LES studies is reproduced. Various simple applications of the BiOMi model (Binomial Objects on Microgrids) are explored, suggesting that well-known phenomena from nature can be captured at low computational cost. These include i) subsampling effects in the convective grey zone, ii) stochastic predator-prey behavior, iii) the down-scale turbulent energy cascade, and iv) simple forms of spatial organization and convective memory. Consequences and opportunities for convective parameterization in next-generation weather and climate models are discussed.

Plain Language Summary

Convective clouds in the Trade wind regions play a crucial role in Earth's climate. The way they interact with the atmospheric circulation is not well understood, and is associated with long-standing problems in weather forecasting and climate prediction. Recent research has suggested that the spatial structure of these cloud fields is a key factor in this problem, and that improving our understanding of such convective cloud patterns is crucial for making progress. This study explores a new model framework for generating such cloud patterns, consisting of populations of convective objects on small grids. The objects are born in a random way, complete a life cycle, and can freely move around on the grid. They can also interact and form larger clusters, obeying certain rules of in-

44 teraction. The way the objects behave and move around features some key innovations
45 compared to previous ecosystem models of this kind. These are introduced to optimize
46 the performance and reduce run time on a computer. Various experiments are conducted
47 to explore the new model, illustrating that observed behavior of convective populations
48 is reproduced. These tests also highlight opportunities created for improving convection
49 in weather and climate models.

50 **1 Introduction**

51 Convective cloud populations in Earth’s atmosphere cover a broad range of spa-
52 tial scales. Their occurrence acts on planetary scales, by persistently covering substan-
53 tial areas of the marine subtropical Trade wind regions. On the other end, individual clouds
54 have dimensions from a few meters up to tens of kilometers. The spatial structure of cu-
55 mulus populations acts on the intermediate (meso)scales and can take many forms, in-
56 cluding random-like distributions (Nair et al., 1998) but also more organized patterns
57 including cold pool structures and convergence lines (Bony et al., 2020).

58 Understanding the spatial structure of cumulus populations is important for var-
59 ious reasons. Global weather and climate models require parameterizations to represent
60 the impact of subgrid-scale processes on the resolved-scale flow. Until recently this still
61 fully included cumulus convection, but ongoing advances in supercomputing have grad-
62 ually created a “grey zone problem” (Wyngaard, 2004; Honnert et al., 2020) in which
63 feasible gridspacings approaches typical neighbor spacings of cumulus clouds (Joseph &
64 Cahalan, 1990). This means convective populations are no longer fully sampled in in-
65 dividual gridboxes, a situation for which existing convective parameterizations need to
66 be adapted (Kwon & Hong, 2017; Brast et al., 2018). A second motivation for study-
67 ing the spatial structure of cumulus populations is the role it plays in the cloud-climate
68 feedbacks (Vogel et al., 2016; Wing et al., 2018).

69 The investigation of spatial patterns in convective cloud fields goes back decades,
70 using large-domain covering observations (Sengupta et al., 1990; Weger et al., 1992; Nair
71 et al., 1998) and more recently also simulations (Tompkins & Semie, 2017; Feingold et
72 al., 2017; Neggers et al., 2019). What is clear is that spatial patterns consist of many
73 individual convective objects. Zooming in on any pattern then leads to ever fewer ele-
74 ments being contained in the shrinking domain of interest. As a result, bulk population

75 averages go from smoothly behaving for a fully sampled population towards binary be-
76 havior for a severely sub-sampled population. The way this happens is strongly affected
77 by clustering (Neggers et al., 2019). Understanding and capturing this transition towards
78 *discrete* behavior, including the role played by spatial organization, is key for develop-
79 ing scale-aware and stochastic convective parameterizations for next-generation weather
80 and climate models.

81 Population models including many small convective elements can give useful new
82 insights into this problem, and potentially provide new pathways for convective param-
83 eterization. For example, rules of interaction can be introduced that reflect known or ob-
84 served physics, by which spatial patterns can emerge freely. Such rules are known from
85 game theory (von Neumann, 1928; von Neumann & Morgenstern, 1944) and cellular au-
86 tomata (von Neumann, 1966; Gardner, 1970). A promising recent example is the lattice
87 or microgrid approach (Khouider et al., 2010; Dorrestijn et al., 2013; Peters et al., 2017),
88 which allows multiple *cloud-scale* structures to evolve naturally and gradually on a 2D
89 grid. Other cloud-scale stochastic frameworks were recently proposed by Hagos et al. (2018)
90 and Sakradzija et al. (2016). One step further down-scale is the Lagrangian particle ap-
91 proach of (Böing, 2016), which tracks a multitude of interacting *sub-cloud* scale elements
92 as they form larger clusters on the grid. Although yielding powerful results, what remains
93 relatively unexplored is how such systems behave in the grey zone, in particular their
94 stochastic and discrete behavior resulting from population subsampling in a too small
95 gridbox. One also wonders if the often considerable computational burden of such multi-
96 object approaches might limit their use as part of a convective parameterization.

97 To gain further insight, in this study a simple toy model is formulated for recre-
98 ating populations of interacting convective objects as distributed over a two-dimensional
99 grid. A defining principle is its fully discrete formulation, aimed at capturing binary be-
100 havior at small population sample sizes. Another primary goal is to achieve a formula-
101 tion that is generally applicable to many types of convection and convective object def-
102 initions, with a computational efficiency that is as high as possible. Object births are
103 represented stochastically as a spatially-aware Bernoulli process, taking the form of a bi-
104 nomial number generator. The same operator is applied to horizontal advection of ob-
105 jects between gridboxes, making this process similarly stochastic and discrete. Object
106 demographics are included, creating age strata and allowing discrete and explicit rep-
107 resentation of life-cycle effects. The formulation of the framework allows for multiple co-

108 existing species, as well as interactions to take place between individual convective ob-
109 jects. The formulation in terms of a Bernoulli process at multiple points in the model
110 considerably enhances the computational efficiency.

111 Section 2 presents the basic formulation of the framework. In Section 3 behavior
112 as implied by the formulation is briefly discussed, including an interpretation of implied
113 scaling behavior, the advection operator, and the computational efficiency of the frame-
114 work. Section 4 demonstrates simple applications of the framework on microgrids, in-
115 cluding both single-species and multi-species setups. This application on microgrids is
116 named BiOMi (Binomial Objects on Microgrids). Opportunities created by introducing
117 simple physics-based rules of object interaction are explored, including predator-prey be-
118 havior, spatial organization and convective memory. Section 5 interprets these results
119 in the context of limitations in the formulation, and compares to other recently proposed
120 stochastic frameworks for atmospheric convection. Section 6 then summarizes the main
121 conclusions and provides an outlook on future steps inspired by this study.

122 **2 Formulation**

123 In this section the framework for describing an evolving population of objects on
124 a discretized grid is defined. At its foundation is a prognostic budget for object num-
125 ber that is discrete and includes various sources and sinks. We adopt the following guid-
126 ing principles in its formulation:

- 127 1. The objects should have a stochastic birth rate and a finite lifespan;
- 128 2. The number of objects present in a gridbox should be both discrete and positive-
129 definite, at any time;
- 130 3. The formulation should be general enough to be applicable to any type of convec-
131 tion.

132 Adopting the first and second principles is motivated by our primary goal of capturing
133 the type of stochasticity that is introduced by the sub-sampling of populations in a too
134 small gridbox. In this “grey-zone” range of resolutions, only a few objects are present
135 at varying stages of their life-cycle, which may lead to binary (i.e. on-off) behavior in
136 their averaged properties. Adopting a discrete approach has direct implications for the
137 formulation of all terms in the number budget.

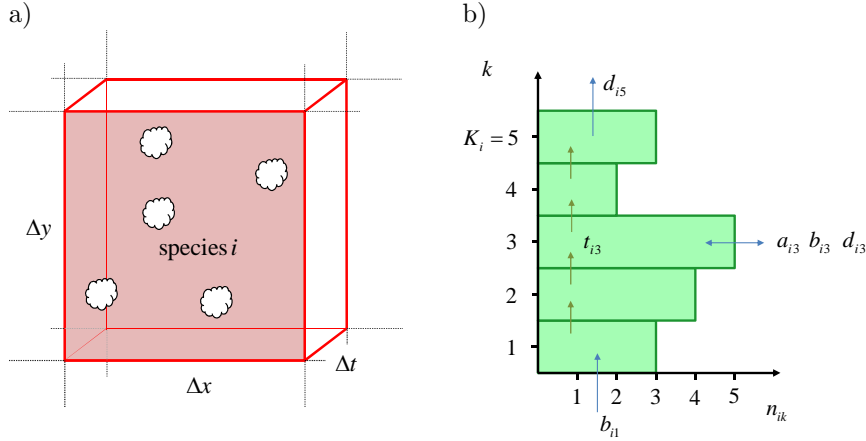


Figure 1. a) Schematic illustration of a population of objects of species i inside a three-dimensional space-time gridbox (red) with square horizontal area $\Delta x \Delta y$ and time-step Δt . b) Schematic illustration of object demographics for a species i with 5 age strata. The blue arrows indicate external sources and sinks of the demographics budget (2), while the green arrows indicate the internal aging process. Variables are explained in Section 2.1.

138 Adhering to the third principle makes it necessary to refrain from defining any clo-
 139 sures that reflect specific physics behavior, as this by definition would make the frame-
 140 work no longer generally applicable. Accordingly, in this section the formulation of such
 141 physical parameterizations is for now left open. However, in Section 4 a few simple ex-
 142 amples will be explored.

143 2.1 A discrete budget for object number

144 Consider a three-dimensional space-time gridbox covering a square horizontal area
 145 $\Delta x \Delta y$ and time-step Δt , as depicted in Fig. 1a. This grid box can contain a population
 146 of objects, potentially consisting of multiple species. The discrete number of objects of
 147 species i is indicated as n_i , with I being the total number of different species. How ex-
 148 actly species are defined is left open at this point, to maintain general applicability of
 149 the framework. Note that the vertical dimension is omitted because the altitude of ob-
 150 jects is not considered in this framework.

151 We now introduce a fourth dimension, which is object age k . The number of ob-
 152 jects of species i in a gridbox can then be written as $n_i(x, y, k, t)$. All four dimensions
 153 are discretized. As a result, the k -dimension introduces a discrete form of object dem-

154 ographics, with k being an integer number indicating an age-stratum. For simplicity all
 155 objects of a species i are assumed to have the same life-span τ_i , by which the number
 156 of age strata K_i is obtained through

$$K_i = \frac{\tau_i}{\Delta t} \quad (1)$$

157 In practice, the chosen time discretization determines how many demographics levels are
 158 maintained. The life times of objects are chosen to be a multiple of Δt , so that K_i is al-
 159 ways an integer number.

160 The final step is to formulate a prognostic budget for each species i at each age level
 161 k . This gives

$$\Delta n_{ik} = b_{ik} - d_{ik} + a_{ik} + t_{ik}. \quad (2)$$

162 The left hand side Δn_{ik} represents the change of n_i at demographics level k per time
 163 step Δt . On the right hand side, b_{ik} and d_{ik} represent changes in n_{ik} due to births and
 164 deaths respectively, a_{ik} represents net advection of objects from neighboring gridboxes,
 165 and t_{ik} represents the process of object aging (demographics). Hereafter, lower-case no-
 166 tation indicates the property of a gridbox, while upper-case notation reflects the inte-
 167 gral or average properties of a much larger domain. To shorten the notation only the species
 168 and age indices i and k are carried as subscripts. Each demographics level k thus has
 169 its own number budget. Note that all terms in (2) are still integer numbers.

170 2.2 Object births as Bernoulli trials

171 The first step in the closure of b_{ik} is to assume that objects of species i have a unique
 172 reference birth rate per unit area and unit time when diagnosed over an infinitely large
 173 area. Let us write this birth rate as \dot{B}_i . Because this rate depends strongly on the def-
 174 inition of the species, for now we assume this birth rate as a given, known property. By
 175 adopting this assumption we follow the recent study of Böing (2016).

176 Given \dot{B}_i , the next step is to consider a finite but still very large reference domain
 177 of horizontal size L in which the population of convective objects is still fully sampled.
 178 The average total number of births of species i within this reference domain during one
 179 time-step, B_i , can then be written as

$$B_i = \dot{B}_i L^2 \Delta t \quad (3)$$

180 A convenient choice of a reference domain would be the whole globe, as this represents
 181 the theoretical upper limit of gridspacing in any General Circulation Model (GCM) used
 182 for global weather and climate prediction. For smaller scale shallow convection one could
 183 also choose a smaller domain, for example the subtropical marine Trade wind region. When
 184 B_i is large and the reference domain is much larger than the individual gridbox, the bi-
 185 nomial sampling approaches the Poisson distribution used by Sakradzija et al. (2015) to
 186 determine stochastic cloud births per gridbox.

187 Discretizing this reference domain at resolution $(\Delta x, \Delta y, \Delta t)$ results in a number
 188 of gridboxes N ,

$$N = \frac{L^2}{\Delta x \Delta y}. \quad (4)$$

189 The total number of birth events in the reference domain, B_i , is spatially distributed over
 190 the grid, yielding an average number of birth events in a single gridbox, μ_i ,

$$\mu_i = \frac{B_i}{N} \quad (5)$$

191 Let us assume for the moment that the spatial distribution is purely random (we will
 192 deviate from this condition later). Then for each of these N birth events the probabil-
 193 ity p that it takes place inside a specific gridbox is

$$p = 1/N. \quad (6)$$

194 Note that probability p is the same for each species, and is purely a property of the dis-
 195 cretized grid. In that sense it introduces scale-awareness, or awareness of the gridspac-
 196 ing. Dependence on species is introduced by B_i .

197 The key step in defining the stochastic birth generator is to assume that the num-
 198 ber of births in an arbitrary gridbox is independent of other gridboxes and timesteps.
 199 This means that object birth events can be considered as single, independent *Bernoulli*
 200 *trials*, associated with a specific success/failure probability p . With that assumption the
 201 full set of B_i birth events that takes place within the reference domain then becomes a
 202 Bernoulli process. Adopting the configuration as defined above this can be written as
 203 the following probability mass function,

$$f_i(b) = \binom{B_i}{b} p^b (1-p)^{(B_i-b)} \quad (7)$$

204 where the binomial coefficient is defined as

$$\binom{B_i}{b} = \frac{B_i!}{b! (B_i - b)!} \quad (8)$$

205 where we assumed for convenience that B_i can be rounded to the nearest integer. Func-
 206 tion $f_i(b)$ can be interpreted as the probability of b births of objects of species i in an
 207 arbitrary gridbox, given a reference domain with properties B_i and p . The mean μ_i of
 208 this binomial distribution, or its expected value, is defined as

$$\mu_i = B_i p, \quad (9)$$

209 which, according to (5) and (6), corresponds exactly to the average number of object births
 210 per gridbox. Note that the actual average number of births on the grid might deviate
 211 from this expected value because each gridbox is sampled independently.

212 In practice, in each space-time gridbox the integer number of births of objects of
 213 species i is determined by randomly sampling the binomial distribution (7). This can
 214 be written as a binomial number generator,

$$b_{i1} = \mathcal{B}(B_i, p), \quad (10)$$

215 where \mathcal{B} represents a single random sample of binomial function f_i . The number of births
 216 b_{i1} thus established for each gridbox can directly be used in budget equation (2), with
 217 subscript $k = 1$ reflecting that all newly born objects enter the demographics array at
 218 the first (youngest) level. The birth rates b_{ik} for $k > 1$ are set to zero for the moment.

219 2.3 Object demographics

220 The introduction of the age dimension k allows representing object life-cycle effects.
 221 At the start of every timestep, objects in one demographics level are *time-shifted* into
 222 the next (older) level. This process is illustrated in Fig. 1b (green arrows). This process
 223 of object aging is included in budget (2) through the operator t_{ik} , defined as

$$t_{ik} = \begin{cases} -n_{ik} & \text{for } k = 1 \\ n_{i,k-1} - n_{ik} & \text{for } 2 \leq k < K_i \\ n_{i,k-1} & \text{for } k = K_i \end{cases} \quad (11)$$

224 The time-shift out of the top (oldest) level represents object death due to old age ,

$$d_{ik} = n_{ik} \text{ for } k = K_i \quad (12)$$

225 Note that this death rate is automatic and discrete, in that it can not create fractional
 226 object numbers. In this aspect it is different from Newtonian relaxation, which would

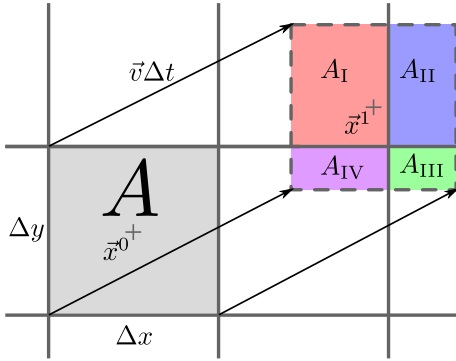


Figure 2. Schematic illustration of overlap between a displaced gridbox and the underlying grid. The arrows represent the displacement over one time step, which is simply the horizontal wind multiplied by the time step duration. Grey crosses mark the mid of the gridbox before and after displacement. See section 2.4 for full description.

227 be an alternative (but non-discrete) formulation. Furthermore, the amount of deaths per
 228 turn is not determined by the amount of objects currently alive, but is directly deter-
 229 mined by the amount of births K_i time steps earlier. The death rates d_{ik} for $k < K_i$,
 230 which represent deaths caused by processes other than ageing, are set to zero for the mo-
 231 ment.

232 2.4 A discrete advection operator

233 If horizontal advection is to be taken into account an advection approach must be
 234 chosen which preserves the total number of objects and their discrete nature. No frac-
 235 tions of objects are permitted.

236 The same Bernoulli process we use to distribute the number of births over a two-
 237 dimensional domain can be used to create a stochastic upwind advection scheme for dis-
 238 crete objects. At the core of this scheme is the assumption that the objects are randomly
 239 spatially distributed within each gridbox. From this assumption the probability of an
 240 object to be advected from one gridbox to another can be determined from the overlap
 241 area as shown in Fig 2. From this principle a conservative advection scheme can be de-
 242 rived that requires 3 sequenced Bernoulli trials per advected gridbox, age strata, and species.

243 The first step is to determine the arrival point \bar{x}^1 of the gridbox mid point after
 244 translation from its original location \bar{x}^0 due to advection by the horizontal wind \vec{v} ,

$$\bar{x}^1 = \bar{x}^0 + \vec{v}\Delta t \quad (13)$$

245 The new gridbox is centered around the arrival point \bar{x}^1 , making it overlap with 4 grid-
 246 boxes. When the displacement is smaller than the grid box there is chance objects will
 247 remain in the original gridbox, if the displacement is larger all objects will move outside.
 248 The overlap areas A_j are labeled in clockwise direction from the topleft one, and obey

$$A = \sum_{j=I}^{IV} A_j \quad (14)$$

249 where $A = \Delta x \Delta y$. For each age level k , we now randomly select objects from the to-
 250 tal number of objects in the original gridbox, n_{ik} , to arrive in each of these four areas
 251 A_j . To this purpose the binomial operator \mathcal{B} as defined before is used,

$$a_{ik,I} = \mathcal{B}(n_{ik}, \frac{A_I}{A}) \quad (15)$$

$$a_{ik,II} = \mathcal{B}(n_{ik} - a_{ik,I}, \frac{A_{II}}{A - A_I}) \quad (16)$$

$$a_{ik,III} = \mathcal{B}(n_{ik} - a_{ik,I} - a_{ik,II}, \frac{A_{III}}{A - A_I - A_{II}}) \quad (17)$$

252 The number of objects advected into A_{IV} is then simply obtained as the residual,

$$a_{ik,IV} = n_{ik} - \sum_{j=I}^{III} a_{ik,j} \quad (18)$$

253 Doing this separately for each age level k means that age is conserved as objects are ad-
 254 vected across the grid

255 For large number of objects per gridbox this discrete advection operator behaves
 256 as a continuous first-order upstream approach with high gradient smoothing and fast dis-
 257 persion. For low object numbers the stochastic nature becomes more visible, with the
 258 mean over all objects no longer smoothly tracking the wind. These aspects will be fur-
 259 ther illustrated in Section 3.2.

260 **2.5 Object interactions**

261 The framework allows introducing interactions between objects in two different ways.
 262 The first option is to make birth probability p appearing in (7) dependent on the pres-
 263 ence of other objects in the vicinity of the gridbox. These could be locally present, in-
 264 side the gridbox, but also in a wider area, covering multiple adjacent gridboxes. The spa-
 265 tial extent of such impacts depends on the physical/dynamical nature of the interaction

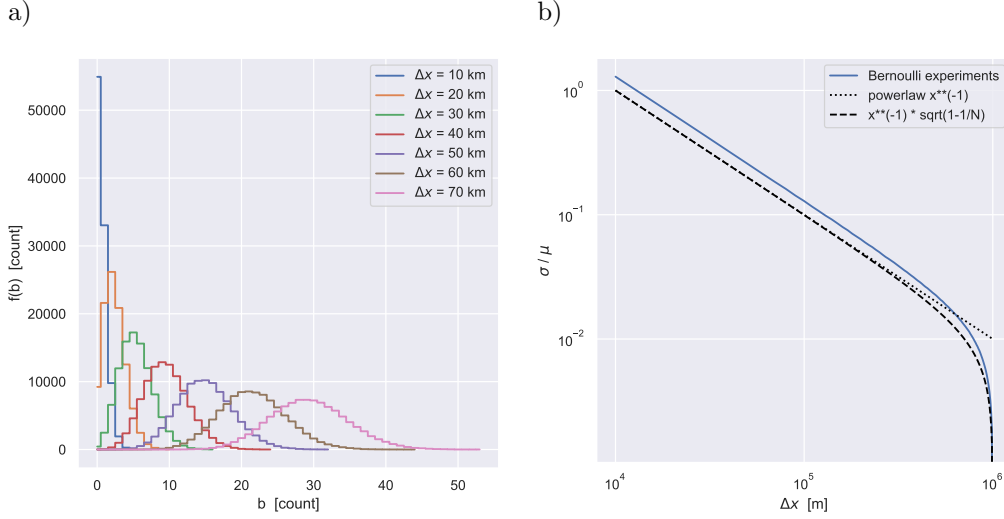


Figure 3. a) Examples of binomial probability density $f(b)$ as defined by (7) for various grid-spacings $\Delta x = \Delta y$, using a birth rate $\dot{B}_i = 10^{-10} \text{ m}^{-2} \text{ s}^{-1}$, a reference domain of size $L = 1000 \text{ km}$ and an integration timestep $\Delta t = 60 \text{ s}$. Results represent 10^6 independent draws. b) Associated functional form of the normalized standard deviation of the binomial distribution σ/μ , as defined by (22). A pure powerlaw (black dotted) and modified powerlaw (black dashed) functional form are also shown, for reference.

266 process of interest. The second option is to make the birth and death rates b_{ik} and d_{ik}
 267 dependent on the presence of other objects. This method is particularly suited to intro-
 268 duce inter-species interactions. For example, predator-prey dynamics can be introduced
 269 by making the death rate of one (prey) species dependent on the presence of another (preda-
 270 tor) species. In Section 4 simple applications of the framework will be demonstrated that
 271 include both forms of interaction between objects.

272 3 Implied behavior

273 With the basic formulation of the framework concluded, some behavior can already
 274 be understood a priori its application in practice. The most relevant of these implied char-
 275 acteristics are discussed in this section.

276 3.1 Stochasticity due to subsampling

277 Describing object births on the grid as independent Bernoulli trials directly con-
 278 trols the behavior of stochasticity in object number at grids spacings at which the pop-

279 ulation is becoming subsampled. This is illustrated in Fig. 3, showing the binomial prob-
 280 ability density function $f(b)$ as defined by (7) for various gridspacings. Both the mean
 281 μ_i and the width $2\sigma_i$ increase with gridspacing Δx , which is expected because p increases
 282 with gridspacing through (6). This results in more births per timestep in larger gridboxes.
 283 A more useful expression of stochasticity is provided by the relative width of the pdf,
 284 σ_i/μ_i . This can be understood by considering the definition of σ_i for the binomial,

$$\sigma_i^2 = B_i p (1-p) = \mu_i \left(1 - \frac{1}{N}\right) \quad (19)$$

285 The standard deviation σ_i normalized by the mean μ_i can then be written as

$$\frac{\sigma_i}{\mu_i} = \mu_i^{-\frac{1}{2}} \left(1 - \frac{1}{N}\right)^{\frac{1}{2}}. \quad (20)$$

286 Note that μ_i carries dependence on both spatial (grid) information and species proper-
 287 ties, because it reflects that B_i births are randomly distributed over a discretized spa-
 288 tial domain. Through (5) this implies a relation for the average neighbor spacing l_i be-
 289 tween objects born in the gridbox within the time-step,

$$l_i = \left(\frac{\Delta x \Delta y}{\mu_i}\right)^{\frac{1}{2}} = \left(\frac{1}{\dot{B}_i \Delta t}\right)^{\frac{1}{2}}. \quad (21)$$

290 Here the neighbor spacing is simply calculated as the square root of the area surround-
 291 ing each object that is free of other objects (on average). Substituting the first part of
 292 (21) for μ_i in (20) then yields the following scaling relation,

$$\frac{\sigma_i}{\mu_i} = \left(\frac{\Delta}{l_i}\right)^{-1} \left(1 - \frac{1}{N}\right)^{\frac{1}{2}} \quad (22)$$

293 where we introduced $\Delta = \sqrt{\Delta x \Delta y}$ to shorten notation. On the right hand side only
 294 the variable l_i depends on the species, through the reference birth rate \dot{B}_i .

295 Each term between brackets in the product on the right hand side of (22) has its
 296 own specific meaning. The first term introduces a powerlaw dependency (with exponent
 297 -1) on the ratio of grid-spacing Δ to the nearest neighbor spacing l_i , with larger val-
 298 ues of (Δ/l_i) suppressing the normalized standard deviation. This reflects that the pop-
 299 ulation of object births of species i is better sampled at larger gridspacings, reducing stochas-
 300 ticity in object number. The second term depends purely on the grid, and acts to bring
 301 the standard deviation to zero in the limit of the grid spacing approaching the reference
 302 domain size.

303 This behavior is illustrated in Fig. 3b, showing the functional dependence of the
 304 normalized standard deviation on gridbox size Δ . In the range of gridspacings typical

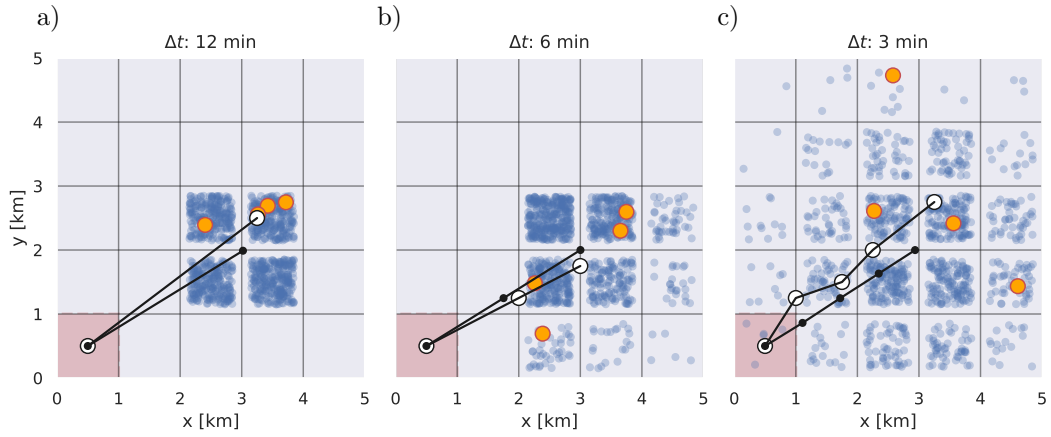


Figure 4. Example of discrete advection of objects on a 5x5 rectangular 1 km grid using the same initial conditions and grid but differing time step. The blue and orange objects behave identically, and differ only in the amount (1000 blue, 4 orange). Note that the individual objects have no specific x and y location within each gridbox, and are only plotted as such for visualization purposes. The red square marks the gridbox in which all objects were initialized at $t=0$, and shown are the locations after 12 minutes of diagonal advection. The black line with small black circles marks the mean location at each time step of the blue objects, the large white circles the mean of the large orange objects.

305 of operational GCMs the second term is almost a constant, because $N \gg 1$. As a re-
 306 sult, the dependence of the normalized standard deviation on grid-spacing approximately
 307 behaves as a powerlaw with exponent -1 . When N approaches 1, the grid in effect be-
 308 comes a slab model, and the variability is squeezed to zero.

309 The powerlaw scaling in the normalized standard deviation as implied by this for-
 310 mulation has recently been encountered in studies of the internal variability of shallow
 311 cumulus cloud size distributions. Neggers et al. (2019) performed subdomain analyses
 312 of unorganized shallow cumulus cloud populations in large-eddy simulations, and found
 313 that the variation across subdomains in the number of convective clouds of a given size
 314 follows scaling relation (22). This agreement provides support for the applicability of the
 315 Bernoulli process for reconstructing such unorganized convective populations.

316

3.2 Discrete advection

317

318

319

320

321

322

323

To illustrate the numerics of the discrete advection operator we run a highly idealized experiment in which all objects are initialized in the same gridbox before being advected diagonally (Fig 4). Objects do not interact with each other or have a life cycle, and all differences between the subplots of Fig 4 are due to the differing number and duration of the timesteps. This testcase was designed to maximize advective diffusion in order to highlight the randomness and discreteness of the stochastic advection operator.

324

325

326

327

328

329

330

331

332

333

334

335

336

337

338

For a large number of objects per gridbox the discrete advection operator behaves as a continuous first-order upstream approach with high gradient smoothing and fast dispersion (small blue dots). But in contrast to a continuous upstream approach, the discrete operator is positive definite and not limited by the Courant–Friedrichs–Lewy condition. How strong and in which direction the dispersion acts depends on the angle of the grid to wind direction, gridbox size, and the timestep. The impact of changing the timestep is shown in Fig. 4, illustrating that changing the timestep can not only affect the strength of the dispersion, but also the direction. As in the continuous analog, increasing resolution reduces diffusion (not shown). Despite this numeric diffusion, the mean over a sufficient number of objects will follow the wind direction closely. For low object numbers the stochastic nature becomes more visible, with the mean over all objects no longer smoothly tracking the wind (large white dots). A side effect of the stochastic nature is that an initially smooth field will become heterogeneous when advected. Similar to the stochastic subsampling this effect is more pronounced for low object numbers (not shown).

339

3.3 Computational viability

340

341

342

Given that efficiency is one of the core concepts of the introduced framework, this subsection briefly discusses the required processing cost and memory requirements of the framework and how they compare to Lagrangian approaches.

343

3.3.1 Processing

344

345

The binomial operator (10) is a cornerstone of the framework, being applied to represent both object births and object advection. A computational benefit of this oper-

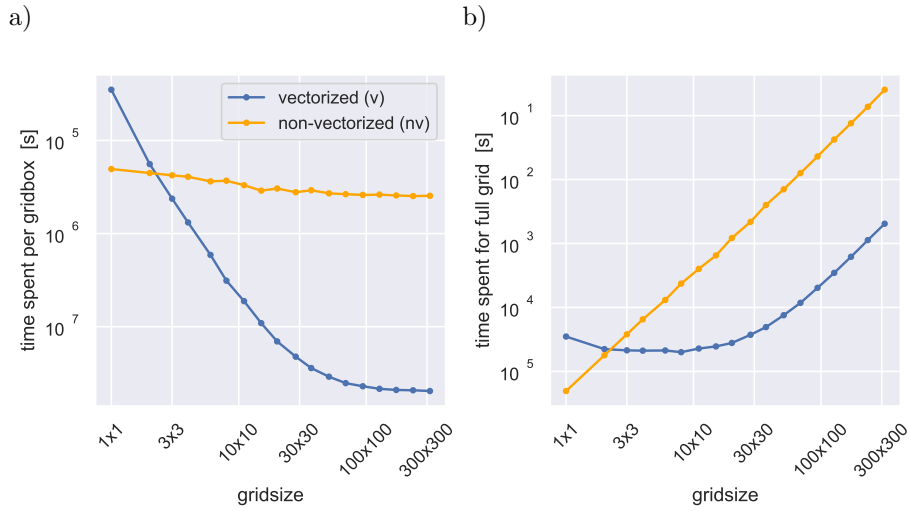


Figure 5. Results of a speed test of the binomial operator (10) as executed in Python on a single Intel i5-6400 2.7 Ghz CPU. a) Time spent per gridbox as a function of gridsize, for a vectorized (*v*) and non-vectorized (*nv*) application. b) Time spent for the full grid.

346 ator is that the operational cost becomes independent of the number of samples drawn
 347 from the distribution. This is a clear distinction from the Lagrangian particle approach
 348 in population dynamical modeling (Böing, 2016), which computes the evolution and move-
 349 ment of each particle individually. As a consequence, the cost of Lagrangian approaches
 350 scales with population size, while that of binomial approaches in principle scales with
 351 gridsize, species number, and age strata.

352 However, thanks to vectorization, the amount of CPU time needed to compute the
 353 binomial sampling need not scale linearly with gridsize, species number, and age strata.
 354 The results of the efficiency test shown in Fig. 5 shed some more light on this possibil-
 355 ity. In the first panel the time spent by the binomial operator for each gridbox is shown
 356 as a function of gridsize. As can be expected, applying the operator in a non-vectorized
 357 way (i.e. a sample at each gridpoint) keeps this cost per gridbox more or less indepen-
 358 dent of gridsize (panel a). As a result, the total cost for the whole grid increases linearly
 359 with the gridsize (panel b). However, while a vectorized application of the binomial op-
 360 erator is slower for a 1x1 grid, it strongly reduces the computational cost in regards to
 361 the gridsize for larger grids. The vectorized version is almost independent of gridsize up
 362 until 30x30, after which the vectorized version is 100× faster than the non-vectorized ver-
 363 sion (panel b). We suspect that the precise gridsize when the cost of the vectorized ver-

364 sion begins to increase with gridsize is related to the CPU memory. The boost in effi-
365 ciency due to the vectorized application, combined with its independence on population
366 size, is what allows the binomial approach to remain computationally viable as part of
367 a convective parameterization, even for microgrids of substantial size. How these ben-
368 efits hold up in practice will vary with hardware and implementation.

369 **3.3.2 Memory**

370 The memory usage of the binomial framework is not determined by the number
371 of objects as would be the case for a Lagrangian approach (Böing, 2016). Instead mem-
372 ory depends linearly on the amount of species, the number of age strata, and the grid-
373 size used. To illustrate memory consumption lets use the advection example shown in
374 Fig. 4. A Lagrangian approach would require the age, x, and y location of each of the
375 the 1004 objects to be tracked individually, resulting in the storage of 3012 float values.
376 Assuming an object lifetime of 24 minutes and a timestep of 12 minutes, as shown in the
377 left subplot of Fig 4, the binomial memory footprint would be $25 \cdot 2 \cdot 2 = 50$ integer
378 values (25 gridboxes, 2 species, 2 age strata). Reducing the timestep to 1 minute while
379 retaining a 24 minute lifetime would increase the memory usage to 1200 integers. An ad-
380 vantage of the discrete framework is that the memory required is static and evenly spread
381 over the grid, which means it can be easily spatially decomposed into individual blocks
382 with the rest of the atmosphere model to be run in parallel. In contrast, the memory us-
383 age of Lagrangian approaches grows and shrinks with the number of particles tracked,
384 and particles moving from one memory domain to the other can complicate the paral-
385 lelization process.

386 **4 Simple applications**

387 In this section the framework is further explored by means of simple experiments
388 with four possible configurations, as applied to grids of small size (“microgrids”). The
389 purpose is not to define ultra-realistic systems; instead, the goal is to explore basic be-
390 havior and highlight opportunities. Achieving a realistic configuration and calibration,
391 including the use of observational datasets, is for now considered a future research topic.
392 Most examples are loosely inspired by atmospheric convection, which is reflected in the
393 definition of the species.

Table 1. Configuration of the four BiOMi experiments discussed in Section 4. Note that Exp 2 is an exception in that it is non-dimensional, age is neglected, and birthrates are derived from differential equations as explained in Subsection 4.2

Setting	Unit	Exp 1	Exp 2	Exp 3	Exp 4
Gridsize		1×1	1×1	15×15	100×100 1000×1000
$\Delta x, \Delta y$	[m]	5000	1	100	100
L	[m]	1000000	5	1000000	1000000
Δt	[s]	60	1/10	60	60
I		10	2	5	1
τ_i	[s]	60	-	600	600
K_i		1	-	10	5
\dot{B}_i	$[\text{m}^{-2} \text{s}^{-1}]$	$\propto (100 \cdot i - 50)^{-2}$	$\dot{B}_1 = g(n_1, n_2)$ $\dot{B}_2 = f(n_1, n_2)$	$\dot{B}_5 = 5 \cdot 10^{-6}$	$\dot{B}_1 = 2 \cdot 10^{-7}$
Interactions		None	Inter-species	Inter-species	Spatial
$(u, v)_{\text{adv}}$	$[\text{m s}^{-1}]$	(0, 0)	(0, 0)	(0.3, 0.2)	(0, 0)
r_f	[m]	-	-	-	300
C_f		-	-	-	2000

394 The framework as applied on microgrids is hereby named *BiOMi* (Binomial Ob-
 395 jects on Microgrids). Using microgrids keeps the examples discussed in this section as
 396 simple and easy to understand as possible. But another important motivation for using
 397 microgrids is the associated high computational efficiency, which could allow its appli-
 398 cation as part of a convection scheme in operational general circulation models used for
 399 weather forecasting and climate prediction.

400 4.1 Exp 1: Single-column random sampler

401 The first experiment demonstrates how the BiOMi framework can be used to in-
 402 troduce stochastic noise in existing convection schemes in operational weather and cli-
 403 mate models. Spectral convection schemes are perhaps best suited to this purpose. This
 404 class of convective parameterizations has been around since the early days of numeri-
 405 cal weather forecasting (Arakawa & Schubert, 1974). A key assumption at the founda-
 406 tion of spectral schemes is the shape of the size distribution of convective elements that
 407 do the vertical transport. In the convective grey zone stochastic noise can be superim-
 408 posed onto this spectrum to represent the impact of subsampling of the population (Neggers,
 409 2015), for which the binomial number generator as proposed in this study can well be
 410 used.

411 As a demonstration a discretized spectrum of convective objects is considered, con-
 412 sisting of a histogram with 10 bins ranging linearly in size from 50 to 950 m. The ref-
 413 erence birth rate of the objects is a power law of of object size with a slope of -2,

$$\dot{B}_i = \lambda (100 \cdot i - 50)^{-2}. \quad (23)$$

414 The proportionality constant λ is scaled such that the birth rate is on average 256 per
 415 gridbox for the 50 m objects. A 1×1 grid is adopted with a grid spacing of 5 km, which
 416 is in the middle of the deep convective grey zone (Arakawa et al., 2011). The reference
 417 domain is 1000 km, and the object distribution is sampled 50 times independently of each
 418 other to evaluate the stochasticity. In these 50 random samplings only the three small-
 419 est and most numerous object species are always present (Fig. 6), with the ratio of sub-
 420 sampling variance to mean number becoming larger for the rarer object species. This
 421 dependence of the stochasticity on size follows the implied behaviour as discussed in Sec-
 422 tion 3.1.

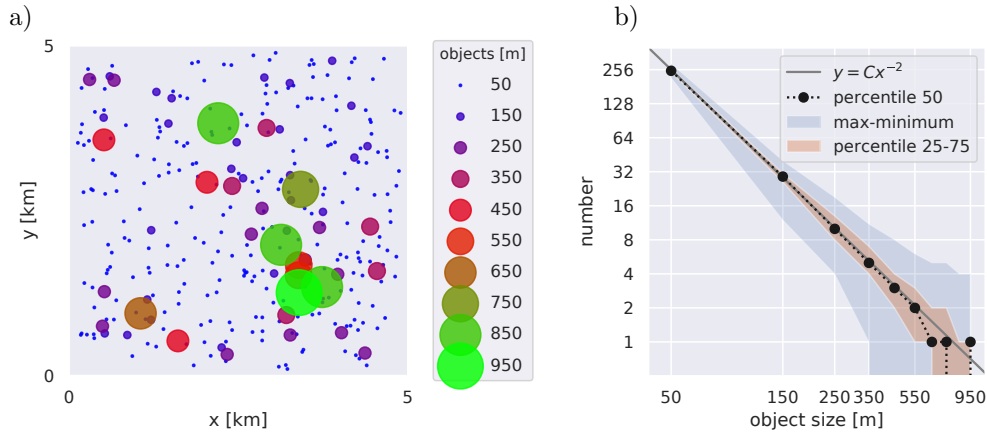


Figure 6. a) Scatter plot illustrating all objects of one of the 50 samples included in subplot b). The x and y position of each object is randomized for visualization. b) Object size distribution statistics of 50 random samplings of objects with decreasing birth rates as detailed in 4.1 with the parameters listed in 1.

423 This simple “offline” experiment thus shows how the binomial framework introduced
 424 in this paper can introduce not only scale-awareness and scale-adaptivity in a spectral
 425 convection scheme (through dependence on the grid spacing), but also stochasticity due
 426 to population subsampling in the grey zone. At the same time, the average number of
 427 objects over the grid is preserved.

428 4.2 Exp 2: Stochastic predator-prey system

429 This experiment is a translation of the continuous predator-prey system of Lotka
 430 (1910, 1920); Volterra (1926) to a discrete analog in which births and deaths are deter-
 431 mined from Bernoulli trials. The intent of this experiment is to highlight the stochas-
 432 tic nature and to illustrate how the individual species can interact while conserving their
 433 discreteness. The predator-prey system was chosen as it a widely known problem that
 434 has been intensively studied in regards to stochasticity (Aguirre et al., 2013) and pre-
 435 viously translated to a system of stochastic cellular automata by Guinot (2002) who stud-
 436 ied under which conditions the behaviour of the cellular automata matches that of the
 437 continuous equations. Predator-prey approaches have also been used in Meteorology to
 438 describe cloud microphysics (Wacker, 1995) and cloud precipitation interactions (Koren
 439 & Feingold, 2011; Pujol & Jensen, 2019).

440 According to the classic formulation of the predator-prey equations, the prey x grows
 441 exponentially with a rate of α but is reduced by the hunting of the predator y which kills
 442 according to the product of prey and predator and β . The predator's growth is linked
 443 to the amount of hunting through δ , and the predator dies off with an exponential de-
 444 cay of strength γ . The equations have a periodic solution around a stable point when
 445 the populations of prey and predator, as well as the four parameters, are all positive.

$$\frac{dx}{dt} = +\alpha x - \beta xy \quad (24)$$

$$\frac{dy}{dt} = -\gamma y + \delta \beta xy \quad (25)$$

446 To switch to our discrete framework we neglect the age dimension and only look
 447 at the total number of prey n_1 and predators n_2 , which simplifies equation (2) to:

$$\Delta n_1 = b_1 - d_1, \quad \Delta n_2 = b_2 - d_2. \quad (26)$$

448 Bernoulli trials are used to determine specific numbers of births and deaths over
 449 Δt by sampling from a N times larger reference domain with the probability $p = 1/N$
 450 that each birth or death of the reference domain occurs in a specific gridbox:

$$b_1 = \mathcal{B}(\alpha n_1 \cdot N \Delta t, p) \quad d_1 = \mathcal{B}(\beta n_1 n_2 \cdot N \Delta t, p), \quad (27)$$

$$b_2 = \mathcal{B}(\delta \beta n_1 n_2 \cdot N \Delta t, p) \quad d_2 = \mathcal{B}(\gamma n_2 \cdot N \Delta t, p). \quad (28)$$

451 Due to the number of deaths being stochastic the populations can become nega-
 452 tive, which we avoid by introducing a limiter. The introduced stochasticity breaks the
 453 even cycle of the continuous solution, visible in the peaks and dips of the discrete prey
 454 in the ensemble quickly dispersing in the example shown in Fig. 7. The discrete nature
 455 is most visible in the less populous predator population. Once the predator population
 456 reaches zero the predator is extinct and can no longer recover. Once extinction occurs
 457 the prey can grow exponentially, as visible in the straight lines leaving the plot domain
 458 in Fig. 7. Note that extinction can occur in the continuous formulation as well when stochas-
 459 tic perturbations are added (Aguirre et al., 2013). The prey can also go extinct, though
 460 it is rarer for the parameters and initial conditions we choose to show.

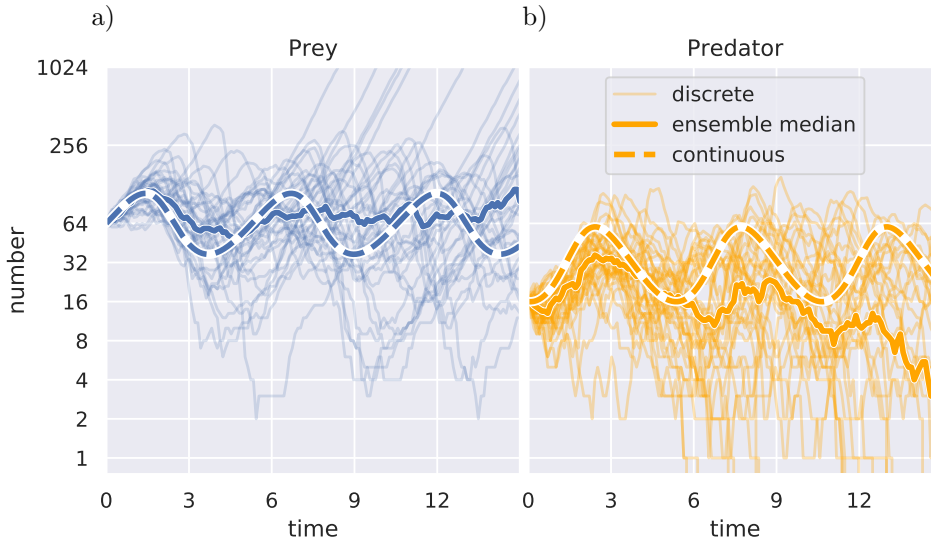


Figure 7. A 36 member of ensemble of the the predator prey system discussed in subsection 4.2 using the parameters $\alpha = 1$, $\beta = 0.03$, $\gamma = 1.5$, $\delta = 0.75$ for equation 24. Initial conditions are 64 (prey) and 16 (predator). Continuous solution is integrated numerically, discrete ensemble is generated using the values listed in table 1.

461

4.3 Exp 3: A down-scale energy cascade

462

463

464

465

466

467

468

469

In the third experiment the model is configured as an ecosystem consisting of five species, without spatial interaction. The goal of this simple experiment is to mimic the down-scale energy cascade typical of atmospheric turbulence (Kolmogorov, 1941a, 1941b; Frisch, 1995). To this purpose each species represents an individual size-class of turbulent structures. Only the largest species experiences births, which is conform the idea that the turbulent energy in an unstable turbulent layer is injected at the largest possible scale. At the end of its life-cycle the object then breaks up into two objects of half its size, which are injected as births in the species-category one size-class smaller,

$$b_{i1}^{\text{casc}} = 2 d_{i+1,10}, \quad (29)$$

470

471

472

473

474

where we used that $K_i = 10$ for all species. This additional birth process is added to the default birth term b_{i1} in budget (2). This process is applied at all scales (species), which in effect establishes a simple form of species interaction in down-scale direction across the spectrum. This process is analogous to the flow of energy across the inertial subrange in turbulence. When an object of the smallest species dies it is simply removed

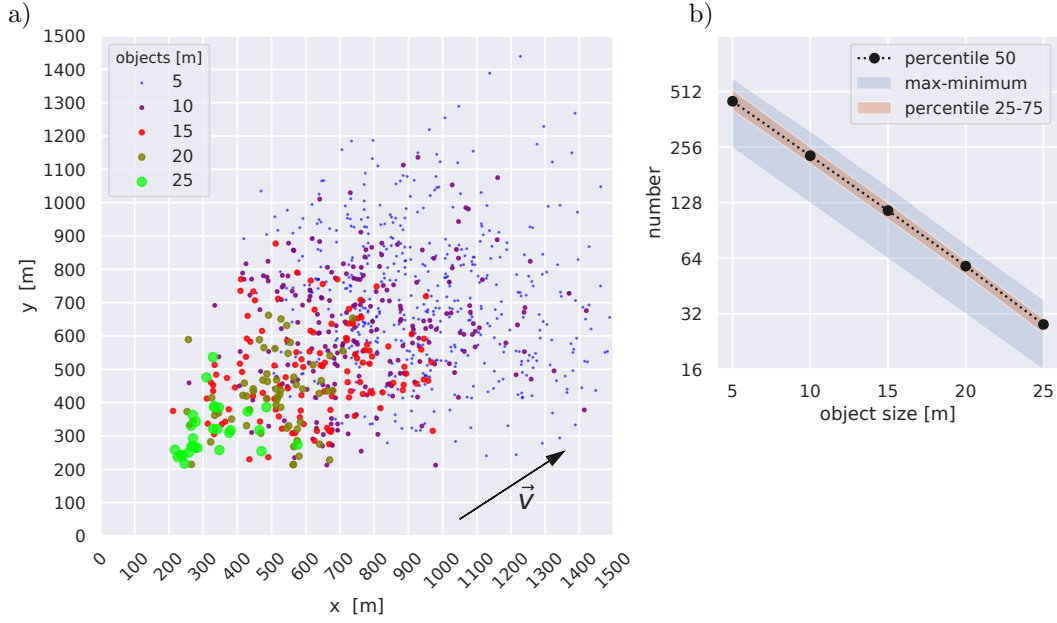


Figure 8. a) Snapshot during an experiment with BiOMi in the five-species energy-cascade configuration as described in Section 4.3 with an arrow showing the wind speed direction advecting the objects. The number of each species per gridbox is shown, with each species having a different size and color. The position of each object within the gridbox is randomized, for visualization. b) Associated size density of object number. The y-axis is plotted in log scale to highlight exponential dependency. The 25-75% range is shaded in red, the maximum and minimum range in blue, and the median is shown as a dotted black line.

475 from the grid, a process analogous to viscous dissipation of turbulent kinetic energy at
 476 molecular scales.

477 To give the experiment another twist, the births of the largest size-class ($i = 5$)
 478 are only allowed to occur in a single specific gridbox (3, 3). For all other species, $\dot{B}_i =$
 479 0 everywhere on the grid. This means the other (smaller) species can only form through
 480 the cascade process described by (29). In addition, a weak mean wind is applied, so that
 481 the objects are slowly advected in the direction marked by the arrow in Fig. 8. As a re-
 482 sult of the advective diffusion illustrated in Subsection 3.2, the population starts to re-
 483 semble a widening plume initiated at a fixed location and being advected down-wind.
 484 This could be a chimney, a forest-fire, or a convective cell creating a slowly dissipating
 485 outflow or anvil cloud. All other settings of the BiOMi model as used for this five-species
 486 experiment are summarized in Table 1.

487 Figure 8a shows a snapshot of the population of objects during this experiment,
 488 an animation of which is also provided as a digital supplement to this paper (Support-
 489 ing Information). Similar to Exp 1 multiple species are present, but they now cover mul-
 490 tiple gridboxes. The results highlight the stochastic nature of both object birth and ad-
 491 vection. The largest objects (green) are born in a single gridbox. As they age, they are
 492 advected by the mean wind, but also break up into two objects half their size (red) when
 493 they complete their life-cycle. This process continues across multiple life-cycles. As a re-
 494 sult, the distance from the birthing-gridbox becomes proportional to age, on average. How-
 495 ever, because advective movement contains a random element, this creates a spreading
 496 plume of particles that “dissipates” when the life cycle of the smallest objects has been
 497 completed. Figure 8b shows the associated size density of object number, which carries
 498 a clear exponential dependence. Such exponential functionality in the spectrum is typ-
 499 ical of a turbulent energy cascade. The spread in object number is caused by the stochas-
 500 tic birth rate and also decreases exponentially with size (i.e. it is constant on the log-
 501 arithmic y-axis). This reflects that all objects have the same life span.

502 **4.4 Exp 4: Spatial organization in a single-species population**

503 The fourth experiment considers only a single species, here assumed to represent
 504 the smallest building block of convection: the short-lived bubble or thermal (Scorer &
 505 Ludlam, 1953; Hernandez-Deckers & Sherwood, 2016; Morrison & Peters, 2018). Sim-
 506 ple rules of spatial interaction are introduced to let thermals respond to each other’s pres-
 507 ence, by which they can collaborate or compete to let larger-scale coherent convective
 508 structures self-organize and emerge on the grid. This behavior introduces convective mem-
 509 ory that acts on time-scales much longer than the life-time of individual objects. The
 510 use of such rules is known from cellular automata, there often referred to as “transition
 511 rules” (Gardner, 1970; Bengtsson et al., 2011).

512 Two rules of interaction are adopted, both working through the probability field
 513 p . These rules reflect atmospheric physics and dynamics, and are inspired by the recent
 514 study by (Böing, 2016). The first rule reflects the “pulsating growth” behavior as ob-
 515 served in individual shallow cumulus clouds in nature, consisting of a series of subsequent
 516 individual pulses (Anderson, 1960; French et al., 1999; Heus et al., 2009). The idea is
 517 that the first pulse breaks down pre-existing instability, favoring subsequent thermals
 518 to thrive and thus form “thermal-chains” (Blyth & Latham, 1993; Damiani et al., 2006;

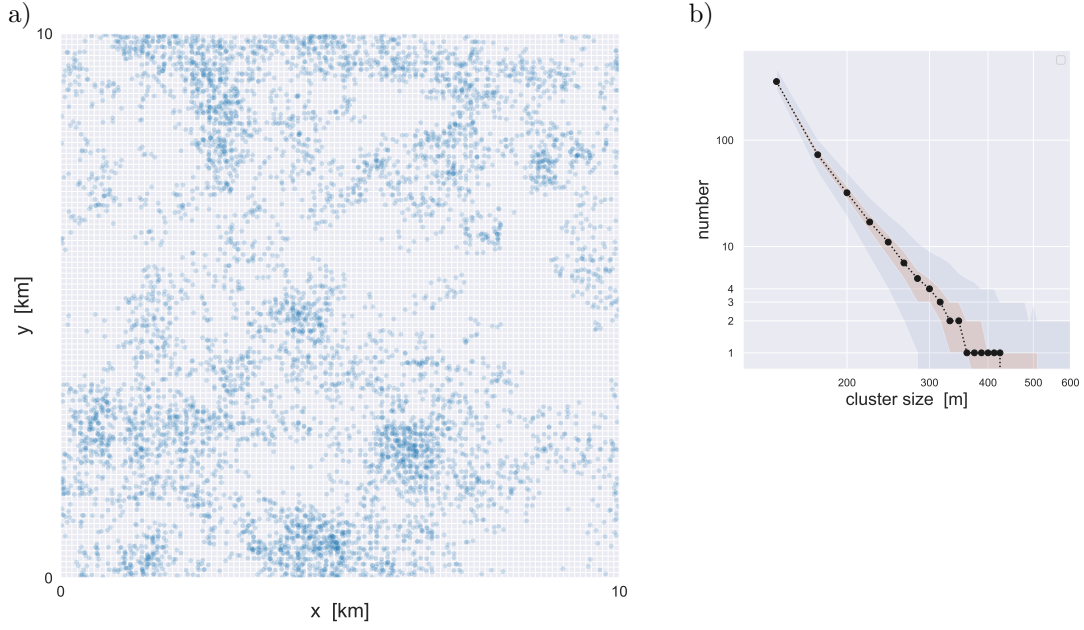


Figure 9. a) Snapshot during an experiment with BiOMi in the single-species configuration with two rules of interaction between objects, as described in Section 4.4. The position of each object within the gridbox is randomized, for visualization. The opacity of each object is 0.2, to highlight clusters. b) Associated size density of cluster number. Log scale is used on both axes for highlighting powerlaw dependency. The 1-99% and 25-75% ranges are shaded blue and red, respectively, while the median is shown as dotted black.

519 Varble et al., 2014). On a microgrid this behavior can simply be introduced by perturb-
 520 ing the p field at locations where objects already exist. The perturbation-field p'_i surround-
 521 ing a single gridpoint containing n_{ik} objects could be modeled as follows,

$$p'_i = C_f f_p \sum_k n_{ik} \quad (30)$$

522 where f_p is a two-dimensional spatial impact field of radius r_f . In this experiment f is
 523 assumed to be cone-shaped,

$$f_p = \begin{cases} 1 - r/r_f & \text{for } r < r_f \\ 0 & \text{for } r \geq r_f \end{cases} \quad (31)$$

524 where r is the distance to the gridpoint of interest, and C_f is a constant of proportion-
 525 ality carrying the efficiency of objects in modifying their environment. The perturba-
 526 tion field p'_i is calculated at every gridpoint and added to the spatially uniform reference
 527 probability $p = 1/N$, yielding a new cumulative field p_c that can be spatially hetero-
 528 geneous.

529 The second rule is a constraint on the perturbed p field which ensures that aver-
 530 aged over the whole grid the mean birth rate always equals \dot{B}_i . To this purpose the new
 531 cumulative probability field including all perturbations, p_c , is suitably normalized,

$$p = \frac{1}{N} \frac{p_c}{\langle p_c \rangle}, \quad (32)$$

532 where the brackets indicate the average over the grid. Comparison to (6) shows that the
 533 grid-dependent probability $1/N$ is multiplied by a spatially varying factor. This means
 534 that while on average the birth rate of the number of objects on the grid B_i remains con-
 535 trolled by external forcings, locally strong deviations can develop in the p field. In ef-
 536 fect, this reduces the probability p in areas where few objects are present. This behav-
 537 ior can loosely be interpreted as environmental deformation caused by convective objects
 538 through for example gravity waves and compensating subsidence (Bretherton & Smo-
 539 larkiewicz, 1989).

540 The model settings for this single-species experiment are also summarized in Ta-
 541 ble 1. An important difference with the third experiment is that the mean wind is zero,
 542 so that objects stay quarantined in their gridbox. In addition, object births are not lim-
 543 ited to a specific single gridbox but can freely occur everywhere on the grid. Thermal
 544 size is implicitly assumed to be on the order of the grid-spacing (~ 100 m). As a result,
 545 any coherent spatial structures resulting from object interactions can be resolved. The
 546 thermals are short-lived while their spatial impact does not exceed beyond $3 \times$ their size.
 547 As a consequence, thermals have to cooperate to let larger-scale structures emerge on
 548 the grid.

549 Animations of Exp 4 for two gridsizes are provided as digital supplements to this
 550 paper (Supporting Information). Figure 9a shows a snapshot of the 100×100 gridsize
 551 experiment at 13 hours after initialization. At this time spatial organization is appar-
 552 ent in the population, featuring dense clusters but also areas that are almost free of ob-
 553 jects. In those areas the probability of birth is very low. By eye this spatial distribution
 554 including both dense and sparsely populated areas is not unlike the organization visi-
 555 ble in high-resolution satellite images of Trade wind cumulus cloud populations (Bony
 556 et al., 2020).

557 Figure 10 shows results from a cluster analysis of this population, using the density-
 558 based GRIDCLUS algorithm (Schikuta, 1996). The clustering threshold is $n > 1$, mean-
 559 ing that only gridboxes are included that have two or more objects in them. Figure 10a

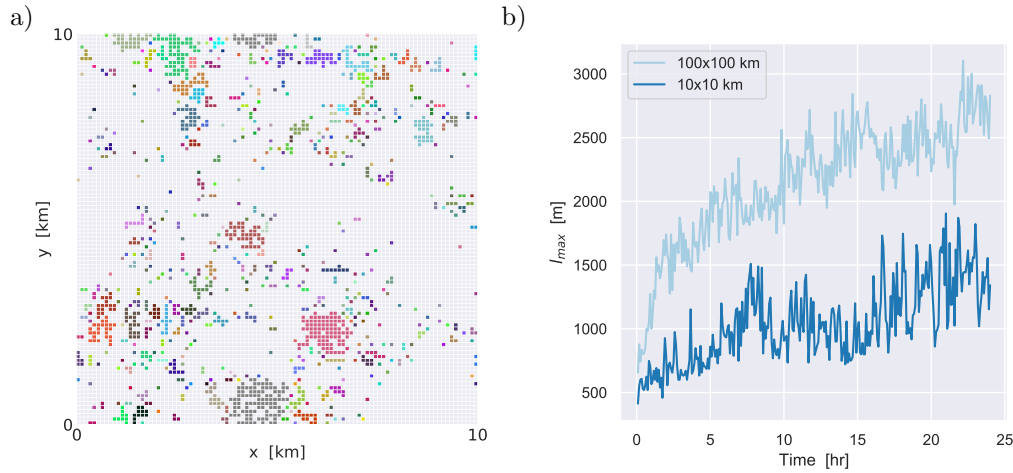


Figure 10. Results of cluster analysis using threshold $n_1 \geq 2$. a) Spatial distribution of the clusters at the last timestep for the experiment with the 10x10 km domain (100x100 gridsize). Each cluster is assigned a unique color. b) Time evolution of the size of the largest cluster on the grid. Results with two domain sizes are shown, 10x10 km (dark blue) and 100x100 km (light blue).

560 shows the resulting clusters on the grid, while Fig. 9b shows the associated size density
 561 of cluster number, with size calculated as the square root of the cluster area. In contrast
 562 to Exp 3 a clear powerlaw dependency is apparent, featuring a negative exponent. This
 563 means that small clusters are very frequent and big clusters are rare. Such powerlaw scal-
 564 ing is frequently observed for shallow cumulus cloud fields in nature (Benner & Curry,
 565 1998; Neggers et al., 2003; Wood & Field, 2011). The widening spread at large cluster
 566 sizes shows that the clusters at those sizes become subsampled, which is a defining fea-
 567 ture of the convective grey zone (Neggers et al., 2019).

568 Another important aspect of the clustering behavior is highlighted by Fig. 10b, show-
 569 ing convective memory on the grid as expressed by the time evolution of the size of the
 570 largest cluster, l_{\max} . Two gridsizes are compared, one with a mesoscale domain size ($D =$
 571 10 km) and one with a macroscale domain ($D = 100$ km). Both domains feature a grad-
 572 ual increase in l_{\max} . However, on the mesoscale domain the growth of l_{\max} is markedly
 573 slower, featuring temporary peaks and failing to grow beyond 1.5 km. This suggests the
 574 cluster growth becomes limited by the domain size. This is not the case for the macroscale
 575 domain, where growth is unimpeded and follows a parabolic evolution (see also the pro-

576 vided animation). What these results suggest is that under simple rules of interaction,
577 convective memory can be created and carried on the grid. Introducing this behavior in
578 convective parameterizations is a long standing ambition that has not yet been achieved
579 (Khairoutdinov & Randall, 2006; Grabowski et al., 2006). If population models on two-
580 dimensional microgrids can solve this problem is a future research topic.

581 **5 Discussion**

582 **5.1 Limitations**

583 The formulation of the framework contains a few important limitations. These were
584 consciously introduced, in order to explore a system that is as low-complexity and trans-
585 parent as possible. However, it is important to consider these limitations and their im-
586 pact on the results. In addition, possible future modifications can be considered that might
587 make the system better reflect realistic conditions.

588 The first limitation is the assumption of a constant object birth rate \dot{B}_i which is
589 sufficient for the purposes of this study. However, what external factors control this birth
590 rate remains a fundamental question and depends strongly on the definition of the species
591 to be represented by the model. In the case of surface-driven convection in a viscous fluid,
592 the number of plumes has been observed to depend on the heating rate at the surface,
593 as expressed by the surface Rayleigh number (Zhong, 2005). Dependence of object birth
594 rates on thermodynamic conditions can be investigated using large-eddy simulations, for
595 example for convective cloud populations (Garrett et al., 2018). Such dependencies can
596 easily be implemented in this framework.

597 The choice to adopt a discrete formulation introduces opportunities but also makes
598 the framework less flexible in some regards. For example, the object lifespan must be
599 a multiple of the timestep, which suggests that adaptive time-stepping would no longer
600 be possible. However, this could be remedied by applying separate timestepping for the
601 microgrid.

602 The use of the binomial advection operator introduces some numerical diffusion which
603 is an unavoidable side effect of any Eulerian advection scheme. The strength and direc-
604 tion of the diffusion is dependent on the horizontal gradients, grid spacing, timestep, and
605 the angle between grid orientation and wind. To achieve a controlled and consistent dif-

606 fusion one could easily combine the advection operator with aspects of the classic Gaus-
 607 sian plume model (Sutton, 1932) that is often used to model dispersion in the atmosphere.

608 The rules of interaction between convective objects as adopted in Exp 4 are still
 609 very simple. While being successful in demonstrating opportunities, important interac-
 610 tions acting in atmospheric moist convection in nature are still missing. These include
 611 i) latent heat effects due to cloud formation, ii) impacts of wind shear on spatial organ-
 612 ization, iii) formation of cold pools due to evaporation of precipitation. Additional rules
 613 can well be added in the system. But before introducing such rules they should be care-
 614 fully calibrated and trained against relevant datasets, for example using machine learn-
 615 ing techniques.

616 5.2 Comparisons to other stochastic frameworks

617 The BiOMi framework as applied in the previous section shares some features with
 618 other recently proposed population models, but also differs in some key aspects. These
 619 similarities, differences and novelties are briefly highlighted here, for reference.

620 The STOMP framework (STOchastic Model for Population dynamics of convec-
 621 tive clouds, Hagos et al. (2018)) is at its core also discrete and stochastic, consisting of
 622 size distributions of convective cells that interact by exchanging "convective pixels". In
 623 contrast to BiOMi's predetermined number *species* that can represent differing convec-
 624 tive objects, STOMP is explicitly defined in terms of cloud size distributions. BiOMi also
 625 differs fundamentally by the inclusion of an explicit age dimension, the use of binomial
 626 sampling to determine births and advection, and the possibility to use a microgrid spa-
 627 tially. As a result, objects in BiOMi can overlap, allowing in principle the representa-
 628 tion of thermal chains that are oriented vertically, as illustrated in Exp4.

629 Recent studies by Stechmann and Hottovy (2016) and Khouider and Bihlo (2019)
 630 proposed stochastic models based on principles from statistical mechanics that represent
 631 convective regimes as phase transitions. BiOMi adheres to this principle, in that spa-
 632 tial patterns associated with convective regimes can freely emerge on the grid under cer-
 633 tain rules of transition. A key conceptual difference concerns the main stochastic bud-
 634 get equation; while these models use integrated humidity, BiOMi considers the evolu-
 635 tion of object number. These interacting objects can also freely move around on the grid,
 636 taking object demographics into account as an additional dimension. This in effect com-

637 bins an object-based approach with a microgrid approach, which is a novelty. The rep-
638 resentation of horizontal movement is another difference, which in BiOMi takes place through
639 stochastic advection instead of stochastic diffusion. Finally, the rules of transition reflect
640 different processes. While in the above studies the rules reflect behavior of cloudy ar-
641 eas as embedded in open- or closed cell stratocumulus, in BiOMi Exp4 the rules reflect
642 the physics and dynamics of individual sub cloud-scale convective thermals in fair-weather
643 cumulus cloud fields.

644 A cloud population model with a stochastic scale-aware birthrate very similar to
645 that of BiOMi was developed by Sakradzija et al. (2015) for use in a shallow convection
646 scheme (Sakradzija et al., 2016; Sakradzija & Klocke, 2018). In their approach the cloud
647 birth rates are sampled from a Poisson distribution instead of a binomial, and further
648 differs from BiOMi in that each cloud has an individual continuous duration and there
649 are no fixed species. For a high number of clouds their approach requires a large amount
650 of memory as the birth time and duration of each cloud is saved individually.

651 **6 Conclusions and outlook**

652 In this study a computationally efficient stochastic binomial framework is formu-
653 lated for representing discrete populations of objects on a two-dimensional grid. A defin-
654 ing feature of the BiOMi framework (Binomial Objects on Microgrids) is its binomial
655 number generator based on a Bernoulli process. This stochastic and scale-aware oper-
656 ator is applied to both object birth and object advection, by which discreteness in ob-
657 ject number is preserved in both processes. A discrete prognostic budget for object num-
658 ber is combined with an age dimension, allowing representation of life-cycle effects and
659 object demographics. In addition, multiple co-existing species can be represented, mak-
660 ing the framework suitable for multiple modes of application. Interactions between ob-
661 jects can be introduced in various ways, by adopting concepts from game theory and cel-
662 lular automata. Finally, due to its reliance on binomial sampling the BiOMi system is
663 also computationally cheap to operate.

664 The BiOMi framework is tested and explored in various simple configurations, de-
665 signed to reflect key aspects of atmospheric turbulence and convection. This yielded the
666 following main conclusions:

- 667 • The binomial number generator is effective in introducing stochasticity in object
668 number due to population subsampling in the convective grey zone;
- 669 • The binomial operator also introduces stochasticity in advection of objects between
670 gridboxes;
- 671 • The framework can successfully reproduce key characteristics of the classic predator-
672 prey problem while preserving discreteness and introducing stochastic variations;
- 673 • Behavior as observed in nature can be reproduced by the system, including i) the
674 down-scale energy cascade in atmospheric turbulence, and ii) spatial organization
675 in convective cloud populations resulting from interactions between objects;
- 676 • The arrangement of binomially generated populations on a microgrid is a form of
677 convective memory, evolving on timescales much longer than the lifespan of in-
678 dividual objects;
- 679 • The computational efficiency is high enough to allow application as part of con-
680 vection schemes in operational weather and climate models.

681 While the framework has many possible applications, its potential use as part of
682 a convective parameterization for weather and climate models has always been a primary
683 motivation behind this study. These opportunities are further explored in an ongoing
684 related study, in which the BiOMi system as applied to a population of single-sized, short-
685 lived but interacting convective thermals as explored in Exp 4 is implemented in a dis-
686 cretized spectral convection scheme ($ED(MF)^n$, Neggers (2015)). BiOMi then acts to pro-
687 vide cluster size densities that emerge on its microgrid, replacing one of the existing clo-
688 sures at the foundation of the scheme. In effect, this equips $ED(MF)^n$ with subgrid con-
689 vective memory and introduces awareness of spatial organization - both longstanding bot-
690 tlenecks in convective parameterization. For testing the $ED(MF)^n$ -BiOMi system is im-
691 plemented as a subgrid transport scheme in a simplified circulation model and explored
692 for prototype cumulus cases. Impacts on the onset of precipitation in diurnal cycles of
693 continental convection are investigated, as well as behavior in the range of resolutions
694 spanning the convective grey zone.

695 BiOMi offers further opportunities when applied within GCM gridboxes. Firstly,
696 existing convection schemes can be equipped with the 1D random sampler as explored
697 in Exp 1 to introduce stochastic noise in the grey zone. Secondly, the microgrid can be
698 used to make surface-atmosphere interactions more sophisticated. For example, aware-

699 ness of small-scale surface heterogeneity can be introduced by coupling the BiOMi mi-
 700 crogrid to similarly high-resolution maps of surface properties. Convective triggering can
 701 then respond in areas which are known to affect this process, such as mountains or ar-
 702 eas of different vegetation.

703 **Acknowledgments**

704 This research was supported by the U.S. Department of Energy’s Atmospheric System
 705 Research, an Office of Science Biological and Environmental Research program, under
 706 grant DE-SC0017999. We thank Brian Mapes, Timothy Garrett and Steve Sherwood for
 707 discussions on early versions of the binomial framework, and Andreas Griewank for ad-
 708 vice related to the framework definitons. The BiOMi code is publicly accessible through
 709 GitHub at <https://github.com/pgriewank/BioMi>. Animations of Exp 3 and Exp 4 with
 710 the BiOMi framework as discussed in Section 3 are provided as Supporting Information
 711 to this publication.

712 **References**

- 713 Aguirre, P., González-Olivares, E., & Torres, S. (2013). Stochastic predator–prey
 714 model with allee effect on prey. *Nonlinear Analysis: Real World Applica-*
 715 *tions*, *14*(1), 768 - 779. Retrieved from [http://www.sciencedirect.com/](http://www.sciencedirect.com/science/article/pii/S1468121812001575)
 716 [science/article/pii/S1468121812001575](http://www.sciencedirect.com/science/article/pii/S1468121812001575) doi: [https://doi.org/10.1016/](https://doi.org/10.1016/j.nonrwa.2012.07.032)
 717 [j.nonrwa.2012.07.032](https://doi.org/10.1016/j.nonrwa.2012.07.032)
- 718 Anderson, C. E. (1960). A Study of the Pulsating Growth of Cumulus Clouds. *Dis-*
 719 *sertation. Massachusetts Institute of Technology.*
- 720 Arakawa, A., Jung, J.-H., & Wu, C.-M. (2011). Toward unification of the multi-
 721 scale modeling of the atmosphere. *Atmospheric Chemistry and Physics*, *11*(8),
 722 3731–3742. Retrieved from [https://www.atmos-chem-phys.net/11/3731/](https://www.atmos-chem-phys.net/11/3731/2011/)
 723 [2011/](https://www.atmos-chem-phys.net/11/3731/2011/) doi: 10.5194/acp-11-3731-2011
- 724 Arakawa, A., & Schubert, W. H. (1974). Interaction of a cumulus cloud ensemble
 725 with the large-scale environment, Part I. *J. Atmos. Sci.*, *31*, 674-701.
- 726 Bengtsson, L., Körnich, H., Källén, E., & Svensson, G. (2011). Large-scale
 727 dynamical response to subgrid-scale organization provided by cellular au-
 728 tomata. *Journal of the Atmospheric Sciences*, *68*(12), 3132-3144. doi:
 729 [10.1175/JAS-D-10-05028.1](https://doi.org/10.1175/JAS-D-10-05028.1)

- 730 Benner, T. C., & Curry, J. A. (1998). Characteristics of small tropical cumulus
 731 clouds and their impact on the environment. *Journal of Geophysical Research:*
 732 *Atmospheres*, 103(D22), 28753-28767. doi: 10.1029/98JD02579
- 733 Blyth, A. M., & Latham, J. (1993). Development of ice and precipitation in New
 734 Mexican summertime cumulus clouds. *Quarterly Journal of the Royal Meteorolo-*
 735 *gical Society*, 119(509), 91-120. doi: 10.1002/qj.49711950905
- 736 Böing, S. J. (2016). An object-based model for convective cold pool dynamics.
 737 *Mathematics of Climate and Weather Forecasting*(1). doi: 10.1515/mcwf-2016
 738 -0003
- 739 Bony, S., Schulz, H., Vial, J., & Stevens, B. (2020). Sugar, gravel, fish, and flow-
 740 ers: Dependence of mesoscale patterns of trade-wind clouds on environmen-
 741 tal conditions. *Geophysical Research Letters*, 47(7), e2019GL085988. doi:
 742 10.1029/2019GL085988
- 743 Brast, M., Schemann, V., & Neggers, R. A. J. (2018). Investigating the Scale
 744 Adaptivity of a Size-Filtered Mass Flux Parameterization in the Gray Zone
 745 of Shallow Cumulus Convection. *Journal of the Atmospheric Sciences*, 75(4),
 746 1195-1214. doi: 10.1175/JAS-D-17-0231.1
- 747 Bretherton, C. S., & Smolarkiewicz, P. K. (1989). Gravity Waves, Compensating
 748 Subsidence and Detrainment around Cumulus Clouds. *Journal of the At-*
 749 *mospheric Sciences*, 46(6), 740-759. doi: 10.1175/1520-0469(1989)046<0740:
 750 GWCSAD>2.0.CO;2
- 751 Damiani, R., Vali, G., & Haimov, S. (2006). The Structure of Thermals in Cumulus
 752 from Airborne Dual-Doppler Radar Observations. *Journal of the Atmospheric*
 753 *Sciences*, 63(5), 1432-1450. doi: 10.1175/JAS3701.1
- 754 Dorrestijn, J., Crommelin, D. T., Biello, J. A., & Böing, S. J. (2013). A data-
 755 driven multi-cloud model for stochastic parametrization of deep convection.
 756 *Philosophical Transactions of the Royal Society A: Mathematical, Physical and*
 757 *Engineering Sciences*, 371(1991), 20120374. doi: 10.1098/rsta.2012.0374
- 758 Feingold, G., Balsells, J., Glassmeier, F., Yamaguchi, T., Kazil, J., & McComiskey,
 759 A. (2017). Analysis of albedo versus cloud fraction relationships in liquid water
 760 clouds using heuristic models and large eddy simulation. *Journal of Geophysi-*
 761 *cal Research: Atmospheres*, 122(13), 7086-7102. doi: 10.1002/2017JD026467
- 762 French, J. R., Vali, G., & Kelly, R. D. (1999). Evolution of small cumulus clouds in

- 763 Florida: observations of pulsating growth. *Atmospheric Research*, *52*, 143-165.
 764 doi: doi:10.1016/S0169-8095(99)00024-1
- 765 Frisch, U. (1995). *Turbulence: The legacy of a. n. kolmogorov*. Cambridge University
 766 Press. doi: 10.1017/CBO9781139170666
- 767 Gardner, M. (1970). Mathematical Games - The Fantastic Combinations of John
 768 Conway's New Solitaire Game 'Life'. *Scientific American*, *223*, 120–123. doi:
 769 10.1038/scientificamerican1070-120
- 770 Garrett, T. J., Glenn, I. B., & Krueger, S. K. (2018, Aug). Thermodynamic
 771 constraints on the size distributions of tropical clouds. *Journal of Geo-*
 772 *physical Research: Atmospheres*, *123*(16), 8832–8849. Retrieved from
 773 <https://dx.doi.org/10.1029/2018JD028803> doi: 10.1029/2018jd028803
- 774 Grabowski, W. W., Bechtold, P., Cheng, A., Forbes, R., Halliwell, C., Khairoutdi-
 775 nov, M., ... Xu, K.-M. (2006). Daytime convective development over land: A
 776 model intercomparison based on LBA observations. *Quarterly Journal of the*
 777 *Royal Meteorological Society*, *132*(615), 317-344. doi: 10.1256/qj.04.147
- 778 Guinot, V. (2002, 06). Modelling using stochastic, finite state cellular automata:
 779 Rule inference from continuum models. *Applied Mathematical Modelling*, *26*,
 780 701-714. doi: 10.1016/S0307-904X(01)00078-6
- 781 Hagos, S., Feng, Z., Plant, R. S., Houze Jr., R. A., & Xiao, H. (2018). A stochas-
 782 tic framework for modeling the population dynamics of convective clouds.
 783 *Journal of Advances in Modeling Earth Systems*, *10*(2), 448-465. Retrieved
 784 from [https://agupubs.onlinelibrary.wiley.com/doi/abs/10.1002/](https://agupubs.onlinelibrary.wiley.com/doi/abs/10.1002/2017MS001214)
 785 [2017MS001214](https://agupubs.onlinelibrary.wiley.com/doi/abs/10.1002/2017MS001214) doi: 10.1002/2017MS001214
- 786 Hernandez-Deckers, D., & Sherwood, S. C. (2016). A Numerical Investigation of Cu-
 787 mulus Thermals. *Journal of the Atmospheric Sciences*, *73*(10), 4117-4136. doi:
 788 10.1175/JAS-D-15-0385.1
- 789 Heus, T., Jonker, H. J. J., Van den Akker, H. E. A., Griffith, E. J., Koutek, M., &
 790 Post, F. H. (2009). A statistical approach to the life cycle analysis of cumu-
 791 lus clouds selected in a virtual reality environment. *Journal of Geophysical*
 792 *Research: Atmospheres*, *114*(D6). doi: 10.1029/2008JD010917
- 793 Honnert, R., Efstathiou, G. A., Beare, R. J., Ito, J., Lock, A., Neggers, R., ... Zhou,
 794 B. (2020). The atmospheric boundary layer and the “gray zone” of turbulence:
 795 A critical review. *Journal of Geophysical Research: Atmospheres*, *n/a*(n/a),

- 796 e2019JD030317. doi: 10.1029/2019JD030317
- 797 Joseph, J. H., & Cahalan, R. F. (1990). Nearest neighbor spacing of fair weather cu-
798 mulus clouds. *J. App. Meteor.*, *29*, 793-805.
- 799 Khairoutdinov, M., & Randall, D. (2006). High-resolution simulation of shallow-
800 to-deep convection transition over land. *Journal of the Atmospheric Sciences*,
801 *63*(12), 3421-3436. doi: 10.1175/JAS3810.1
- 802 Khouider, B., Biello, J., & Majda, A. J. (2010, 03). A stochastic multcloud model
803 for tropical convection. *Commun. Math. Sci.*, *8*(1), 187-216.
- 804 Khouider, B., & Bihlo, A. (2019). A new stochastic model for the boundary layer
805 clouds and stratocumulus phase transition regimes: Open cells, closed cells,
806 and convective rolls. *Journal of Geophysical Research: Atmospheres*, *124*(1),
807 367-386. Retrieved from [https://agupubs.onlinelibrary.wiley.com/doi/](https://agupubs.onlinelibrary.wiley.com/doi/abs/10.1029/2018JD029518)
808 [abs/10.1029/2018JD029518](https://agupubs.onlinelibrary.wiley.com/doi/abs/10.1029/2018JD029518) doi: 10.1029/2018JD029518
- 809 Kolmogorov, A. (1941a). Dissipation of energy in locally isotropic turbulence. *Dokl.*
810 *Akad. Nauk SSSR*, *32*, 16–18.
- 811 Kolmogorov, A. (1941b). The local structure of turbulence in incompressible viscous
812 fluid for very large Reynolds numbers. *Dokl. Akad. Nauk SSSR*, *30*, 301–305.
- 813 Koren, I., & Feingold, G. (2011). Aerosol–cloud–precipitation system as a predator-
814 prey problem. *Proceedings of the National Academy of Sciences*, *108*(30),
815 12227–12232. Retrieved from <https://www.pnas.org/content/108/30/12227>
816 doi: 10.1073/pnas.1101777108
- 817 Kwon, Y. C., & Hong, S.-Y. (2017). A Mass-Flux Cumulus Parameterization
818 Scheme across Gray-Zone Resolutions. *Mon. Wea. Rev.*, *145*(2), 583–598. doi:
819 10.1175/MWR-D-16-0034.1
- 820 Lotka, A. (1910). Contribution to the Theory of Periodic Reaction. *J. Phys. Chem.*,
821 *14*, 271-274.
- 822 Lotka, A. (1920). Analytical Note on Certain Rhythmic Relations in Organic Sys-
823 tems. *Proc. Natl. Acad. Sci. U.S.*, *6*, 410-415.
- 824 Morrison, H., & Peters, J. M. (2018). Theoretical Expressions for the Ascent Rate of
825 Moist Deep Convective Thermals. *Journal of the Atmospheric Sciences*, *75*(5),
826 1699-1719. doi: 10.1175/JAS-D-17-0295.1
- 827 Nair, U. S., Weger, R. C., Kuo, K. S., & Welch, R. M. (1998). Clustering, ran-
828 domness, and regularity in cloud fields: 5. the nature of regular cumulus

- 829 cloud fields. *J. Geophys. Res.: Atmospheres*, 103(D10), 11363–11380. doi:
 830 10.1029/98jd00088
- 831 Neggers, R. A. J. (2015). Exploring bin-macrophysics models for moist convective
 832 transport and clouds. *Journal of Advances in Modeling Earth Systems*, 7(4),
 833 2079–2104. doi: 10.1002/2015MS000502
- 834 Neggers, R. A. J., Griewank, P. J., & Heus, T. (2019). Power-Law Scaling in the
 835 Internal Variability of Cumulus Cloud Size Distributions due to Subsampling
 836 and Spatial Organization. *Journal of the Atmospheric Sciences*, 76(6), 1489–
 837 1503. doi: 10.1175/JAS-D-18-0194.1
- 838 Neggers, R. A. J., Jonker, H. J. J., & Siebesma, A. P. (2003). Size Statistics of
 839 Cumulus Cloud Populations in Large-Eddy Simulations. *Journal of the At-
 840 mospheric Sciences*, 60(8), 1060–1074. doi: 10.1175/1520-0469(2003)60<1060:
 841 SSOCCP>2.0.CO;2
- 842 Peters, K., Crueger, T., Jakob, C., & Möbis, B. (2017). Improved MJO-simulation
 843 in ECHAM6.3 by coupling a Stochastic Multicloud Model to the convection
 844 scheme. *Journal of Advances in Modeling Earth Systems*, 9(1), 193–219.
 845 Retrieved from [https://agupubs.onlinelibrary.wiley.com/doi/abs/
 846 10.1002/2016MS000809](https://agupubs.onlinelibrary.wiley.com/doi/abs/10.1002/2016MS000809) doi: 10.1002/2016MS000809
- 847 Pujol, O., & Jensen, A. (2019). Cloud–rain predator–prey interactions: An-
 848 alyzing some properties of the koren–feingold model and introduction of
 849 a new species-competition bulk system with a hopf bifurcation. *Phys-
 850 ica D: Nonlinear Phenomena*, 399, 86 - 94. Retrieved from [http://
 851 www.sciencedirect.com/science/article/pii/S0167278918301520](http://www.sciencedirect.com/science/article/pii/S0167278918301520) doi:
 852 <https://doi.org/10.1016/j.physd.2019.04.007>
- 853 Sakradzija, M., & Klocke, D. (2018). Physically constrained stochastic shallow
 854 convection in realistic kilometer-scale simulations. *Journal of Advances
 855 in Modeling Earth Systems*, 10(11), 2755–2776. Retrieved from [https://
 856 agupubs.onlinelibrary.wiley.com/doi/abs/10.1029/2018MS001358](https://agupubs.onlinelibrary.wiley.com/doi/abs/10.1029/2018MS001358) doi:
 857 10.1029/2018MS001358
- 858 Sakradzija, M., Seifert, A., & Dipankar, A. (2016). A stochastic scale-aware pa-
 859 rameterization of shallow cumulus convection across the convective gray zone.
 860 *Journal of Advances in Modeling Earth Systems*, 8(2), 786–812. Retrieved
 861 from <https://agupubs.onlinelibrary.wiley.com/doi/abs/10.1002/>

- 2016MS000634 doi: 10.1002/2016MS000634
- Sakradzija, M., Seifert, A., & Heus, T. (2015). Fluctuations in a quasi-stationary shallow cumulus cloud ensemble. *Nonlinear Processes in Geophysics*, 22(1), 65–85. Retrieved from <https://www.nonlin-processes-geophys.net/22/65/2015/> doi: 10.5194/npg-22-65-2015
- Schikuta, E. (1996). Grid-clustering: an efficient hierarchical clustering method for very large data sets. *Proceedings of the 13th International Conference on Pattern Recognition*, 2, 101-105.
- Scorer, R. S., & Ludlam, F. H. (1953). Bubble theory of penetrative convection. *Quarterly Journal of the Royal Meteorological Society*, 79(339), 94-103. doi: 10.1002/qj.49707933908
- Sengupta, S. K., Welch, R. M., Navar, M. S., Berendes, T. A., & Chen, D. W. (1990). Cumulus Cloud Field Morphology and Spatial Patterns Derived from High Spatial Resolution Landsat Imagery. *Journal of Applied Meteorology*, 29(12), 1245-1267. doi: 10.1175/1520-0450(1990)029<1245:CCFMAS>2.0.CO;2
- Stechmann, S. N., & Hottovy, S. (2016). Cloud regimes as phase transitions. *Geophysical Research Letters*, 43(12), 6579-6587. doi: 10.1002/2016GL069396
- Sutton, O. G. (1932). A theory of eddy diffusion in the atmosphere. *Proc. Roy. Soc. London, A*, 135, 143-165.
- Tompkins, A. M., & Semie, A. G. (2017). Organization of tropical convection in low vertical wind shears: Role of updraft entrainment. *Journal of Advances in Modeling Earth Systems*, 9(2), 1046-1068. doi: 10.1002/2016MS000802
- Varble, A., Zipser, E. J., Fridlind, A. M., Zhu, P., Ackerman, A. S., Chaboureaud, J.-P., ... Shipway, B. (2014). Evaluation of cloud-resolving and limited area model intercomparison simulations using TWP-ICE observations: 1. Deep convective updraft properties. *Journal of Geophysical Research: Atmospheres*, 119(24), 13,891-13,918. doi: 10.1002/2013JD021371
- Vogel, R., Nuijens, L., & Stevens, B. (2016). The role of precipitation and spatial organization in the response of trade-wind clouds to warming. *Journal of Advances in Modeling Earth Systems*, 8(2), 843-862. doi: 10.1002/2015MS000568
- Volterra, V. (1926). Variazioni e fluttuazioni del numero d'individui in specie ani-

- 895 mali conviventi. *Mem. Acad. Lincei Roma*, 2, 31-113.
- 896 von Neumann, J. (1928). Zur Theorie der Gesellschaftsspiele. *Math. Ann.*, 100, 295-
897 320. doi: 10.1007/BF01448847
- 898 von Neumann, J. (1966). Theory of Self-Reproducing Automata, A.W. Burks (Ed.).
899 *University of Illinois Press, Urbana, IL.*
- 900 von Neumann, J., & Morgenstern, O. (1944). Theory of games and economic behav-
901 ior. *Princeton University Press.*
- 902 Wacker, U. (1995). Competition of precipitation particles in a model with parame-
903 terized cloud microphysics. *Journal of the Atmospheric Sciences*, 52(14), 2577-
904 2589. Retrieved from [https://doi.org/10.1175/1520-0469\(1995\)052<2577:COPPIA>2.0.CO;2](https://doi.org/10.1175/1520-0469(1995)052<2577:COPPIA>2.0.CO;2) doi: 10.1175/1520-0469(1995)052<2577:COPPIA>2.0.CO;2
- 905 COPPIA>2.0.CO;2 doi: 10.1175/1520-0469(1995)052<2577:COPPIA>2.0.CO;2
- 906 Weger, R. C., Lee, J., Zhu, T., & Welch, R. M. (1992). Clustering, randomness and
907 regularity in cloud fields: 1. theoretical considerations. *Journal of Geophysical*
908 *Research: Atmospheres*, 97(D18), 20519-20536. doi: 10.1029/92JD02038
- 909 Wing, A. A., Reed, K. A., Satoh, M., Stevens, B., Bony, S., & Ohno, T. (2018).
910 Radiative-convective equilibrium model intercomparison project. *Geo-*
911 *scientific Model Development*, 11(2), 793-813. Retrieved from [https://](https://www.geosci-model-dev.net/11/793/2018/)
912 www.geosci-model-dev.net/11/793/2018/ doi: 10.5194/gmd-11-793-2018
- 913 Wood, R., & Field, P. R. (2011). The Distribution of Cloud Horizontal Sizes. *Jour-*
914 *nal of Climate*, 24(18), 4800-4816. doi: 10.1175/2011JCLI4056.1
- 915 Wyngaard, J. C. (2004). Toward Numerical Modeling in the “Terra Incog-
916 nita”. *Journal of the Atmospheric Sciences*, 61(14), 1816-1826. doi:
917 10.1175/1520-0469(2004)061<1816:TNMITT>2.0.CO;2
- 918 Zhong, S. (2005, 07). Dynamics of thermal plumes in three-dimensional isoviscous
919 thermal convection. *Geophysical Journal International*, 162(1), 289-300. doi:
920 10.1111/j.1365-246X.2005.02633.x